Thin Solid Films 697 (2020) 137827

Contents lists available at ScienceDirect

Thin Solid Films

journal homepage: www.elsevier.com/locate/tsf

Comparing C_{60} and C_{70} as acceptor in organic solar cells: Influence of the electronic structure and aggregation size on the photovoltaic characteristics

L. Benatto[a,*], C.F.N. Marchiori[b], T. Talka[c], M. Aramini[c], N.A.D. Yamamoto[d], S. Huotari[c], L.S. Roman[a], M. Koehler[a]

[a] Department of Physics, Federal University of Paraná, C.P 19044, 81531-980, Curitiba-PR, Brazil
[b] Department of Chemistry – Ångström Laboratory, Uppsala University, Lägerhyddsvägen 1, Box 538, Uppsala 751 21, Sweden
[c] Department of Physics, University of Helsinki, P.O. Box 64 Helsinki, FI- 00014 Finland
[d] Department of Electrical Engineering and Computer Sciences, University of California, Berkeley, Berkeley, California 94720, United States

ARTICLE INFO

Keywords:
Organic photovoltaics
Fullerenes
Density functional theory
Transfer matrix method
Aggregation size

ABSTRACT

The difference in aggregation size of the C_{60} and C_{70} fullerenes affect the photovoltaic performance of devices assembled in the so-called bilayer architecture with poly[2,7-(9,9- dioctyl- dibenzosilole)- alt-4,7- bis(thiophen-2-yl)benzo- 2,1,3- thiadiazole] (PSiF-DBT) as the electron donor material. Despite the better performance of the C_{70} devices, which is related to the high absorption coefficient in the visible range and the superior charge transport properties, the short-circuit current variation upon annealing treatment at 100 °C is approximately twice bigger when the C_{60} is the acceptor. We attribute this effect to the tendency of C_{60} in form smaller aggregate domains relatively to the C_{70}. The increased roughness on the polymeric surface after annealing results in an enhanced donor/acceptor contact area and assists the fullerene diffusion deeper inside the polymeric layer. This effect leads to a better mixing between donor and acceptor species and create a interpenetrating layer close to the so-called bulk heterojunction. Since C_{60} forms smaller aggregates, this mechanism is more pronounced for this molecule. Therefore, a significant variation in the performance of the C_{60} devices is observed after this kind of treatment. Density Functional Theory calculations of the potential energy of interaction between two fullerene molecules and X-Ray measurements gives evidences to support this idea. In addition, combining spectrally resolved external quantum efficiency measurements with optical modeling our results also indicate the occurrence of the bilayer interfacial mixing for PSiF-DBT/C_{60}.

1. Introduction

Organic photovoltaics (OPVs) are very promising compared to inorganic based devices due to several advantages such as light weight, flexibility and fast processing [1] as well as the possibility of printing large areas using, for instance the roll-to-roll technique [2–4] . Usually, a p-type semiconductor is blended with a n-type material that acts as the electron acceptor, such as the functionalized fullerenes in the bulk heterojunction (BHJ) devices configuration [5] . However, to gain insights on the key processes that underlie the energy conversion, one interesting approach is to process these materials in separated layers configuring the bilayer geometry [6–11] . Furthermore, fullerenes (C_{60} and C_{70}) [12] are significantly cheaper than its functionalized analogues.

Fullerenes (C_{60} and C_{70}) were discovered in 1985 by Kroto et al. [13], Hare et al. [14] and since the discovery of the ultrafast electron transfer from a photoexcited polymer to the fullerene by Sariciftci et al. [15] these materials have been widely used as electron acceptor in organic solar cells [16–18] . C_{60} is composed of twelve pentagons and 20 hexagons of carbon arrange and in a spherical shape with diameter around 1 nm; its symmetry is the icosahedral point group I_h. C_{70} has additional hexagonal rings along an equatorial line, and thus is more elongated belonging to the D_{5h} symmetry [19] .

Kazaoui et al. [20] studied the charge transfer (CT) states based on the absorbance and photocurrent spectra of C_{60} and C_{70} materials. Although the 0–0 electronic transitions are observed at very similar energies, (Frenkel excitons, exciton at the same molecule, 1.85 and 1.82 eV, respectively) the CT exciton (separated electron and hole over neighboring molecules) are observed at lower energies in C_{70} (CT_1 at 2.35 and 1.85 eV for C_{60} and C_{70}, respectively). The reported photocurrent spectra show that the photo-carrier generation is more efficient in C_{70} when compared to C_{60}, which may contribute to improve the

* Corresponding author.
E-mail address: lb08@fisica.ufpr.br (L. Benatto).

https://doi.org/10.1016/j.tsf.2020.137827
Received 27 September 2019; Received in revised form 13 December 2019; Accepted 26 January 2020
Available online 28 January 2020

overall power conversion efficiency of organic solar cells. In addition, C_{70} also presents a broader absorption spectrum which can improve the power conversion efficiency (PCE) of organic solar cells, especially if combined with a low-band-gap copolymer (see Ref [21]. and references therein).

Si-bridging copolymers were tested as active layer as it has distinct properties when compared to their carbon-bridging analogues [22–25] . Several authors have studied the effect of the silole group on molecular orbital shapes, energies or the interaction between the polymeric chains [24] . Specifically, the poly[2,7-(9,9-dioctyl-dibenzosilole)-alt-4,7-bis (thiophen-2-yl)benzo-2,1,3-thiadiazole] (PSiF-DBT) has been used as active layer in hybrid [26,27], inverted [28] or BHJ solar cells [22,24,29] . The PSiF-DBT copolymer features by its good thermal stability [30] and high degree of charge delocalization, leading to a high field-effect mobility around 1×10^{-3} $cm^2/(V.s)$ which decreases the series resistance (R_s) in photovoltaic devices [22] .

Nevertheless, the power conversion efficiency of polymeric photovoltaic devices also depends on the polymer's band-gap and on the energy levels alignment between donor (polymer) and acceptor (fullerene). Using this perspective, Zhou et al. proposed that an ideal copolymer for photovoltaic applications must have a highest occupied molecular orbital (HOMO) level at around 5.4 eV and a lowest unoccupied molecular orbital (LUMO) level at around 3.9 eV [21,31] . The PSiF-DBT fits quite well those requirements since it has a HOMO energy level at 5.40 eV and a LUMO energy level at 3.60 eV [22,30] . As a consequence, the PSiF-DBT has a broad absorption spectrum that covers the most intense part of the solar emission spectrum.

In this work, we report how differently aggregation properties of C_{60} and C_{70} fullerenes affect the photovoltaic performance of devices assembled in the so-called bilayer architecture as depicted in Fig. 1. The devices were prepared with PSiF-DBT as the electron donor material and a comparative study of devices comprising C_{60} or C_{70} as the electron accepting layer was performed from both experimental and theoretical perspectives. Despite the better performance of the C_{70} devices, the variation of short circuit current (J_{SC}) after the annealing treatment at 100 °C is approximately twice greater when the C_{60} is the acceptor. We attribute this effect to the fact that the C_{60} forms smaller aggregate domains relative to the C_{70}. Density Functional Theory (DFT) calculations of the potential energy of interaction between two fullerene molecules and X-Ray measurements gives evidences to support this idea. The differences in the size of the aggregate domains interfere in the diffusion of the acceptor into the polymeric layer upon annealing. As a consequence, the devices containing C_{60} have a higher degree of mixing at the polymer/fullerene interface in comparison to devices with C_{70} (that tends to preserve their bilayer-like character even after the thermal treatment). This result is verified by combining spectrally resolved external quantum efficiency measurements (EQE) with optical modeling as an indicator of bilayer interfacial mixing [32].

2. Experimental, optical modeling and computational procedures

2.1. Experimental methods

Photovoltaic devices were fabricated using a commercial indium tin oxide (ITO) coated onto glass substrates (Delta Technologies, with sheet resistance 5–15 Ω), which were previously cleaned in ultra-sonic bath with acetone and isopropanol. To improve the wettability an additional treatment was done in ultra-sonic bath with methanol. A poly(3,4-ethylenedioxythiophene):poly(styrenesulfonate) (PEDOT:PSS - purchased from Sigma-Aldrich, 1.3 wt% dispersion in H_2O, conductive grade) layer were spin-coated and annealed at 100 °C for 40 min in vacuum. The active layer was spin coated from a PSiF-DBT, purchased from Lumtec Technology Corp with number average molecular weight (Mn) > 10 000 g mol^{-1}. The polymer layer was deposited by spin-coating from solution prepared in o-dichloro-benzene [33], and after the film deposition, annealed at 100 °C or 200 °C for 20 min in vacuum. After the polymeric layer be annealed, the acceptor layer was thermally evaporated forming a film with 30 nm of thickness. As mentioned before, two different fullerenes as electron acceptor layer were considered, C_{60} and C_{70}, both purchased from Sigma-Aldrich. Finally, a 70 nm thickness of aluminum were evaporated using a shadow mask to form the metallic electrode. Both evaporations were done under a vacuum pressure of 5×10^{-4} Pa. After the complete assembled, the devices were post-annealed at 70 °C for 5 min in vacuum to ensure a deep polymer:fullerene contact. Current-voltage characteristics were acquired with a solar simulator (lamp) with AM 1.5 G filters. The polymer absorption spectrum was collected directly from the film deposited on quartz substrate in a Shimadzu UV-2450 spectrophotometer, using quartz/air as the reference, in the range of 190–800 nm and the fullerenes spectra were obtained from the film deposited onto glass substrate using glass/air as the reference. X-ray diffraction was performed on a PANalytical X'Pert PRO MPD instrument using Cu Kα radiation. Debye-Scherrer geometry in a grazing incidence mode was exploited by fixing the incident wave at an angle of 2.5° with respect to the sample surface. Diffraction patterns were collected between 2θ = 7–24° on samples annealed at 70° for 15 min. Atomic Force Microscopy (AFM) images were obtained from a Shimadzu SPM-9700. AFM intermittent mode (dynamic mode) measurements were carried out in air using a standard silicon doped cantilevers (metallic reflex coating, nominal spring constants k ~ 21–78 N/m and resonant frequency ω_0 ~ 250–390 kHz).

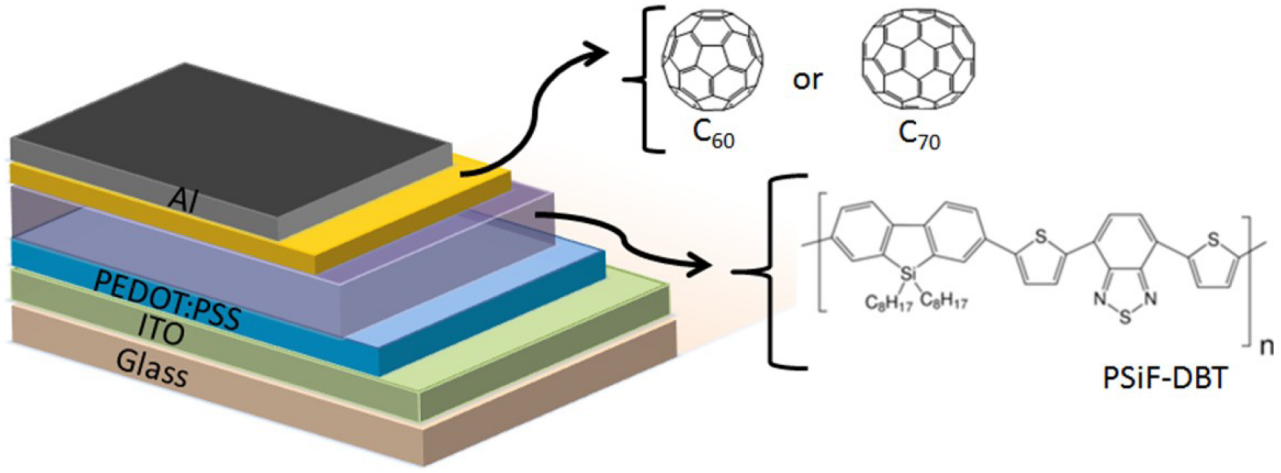

Fig. 1. – Schematic representation of the bilayer device fabricated with PSiF-DBT as electron donor and the electron acceptor materials C_{60} and C_{70}.

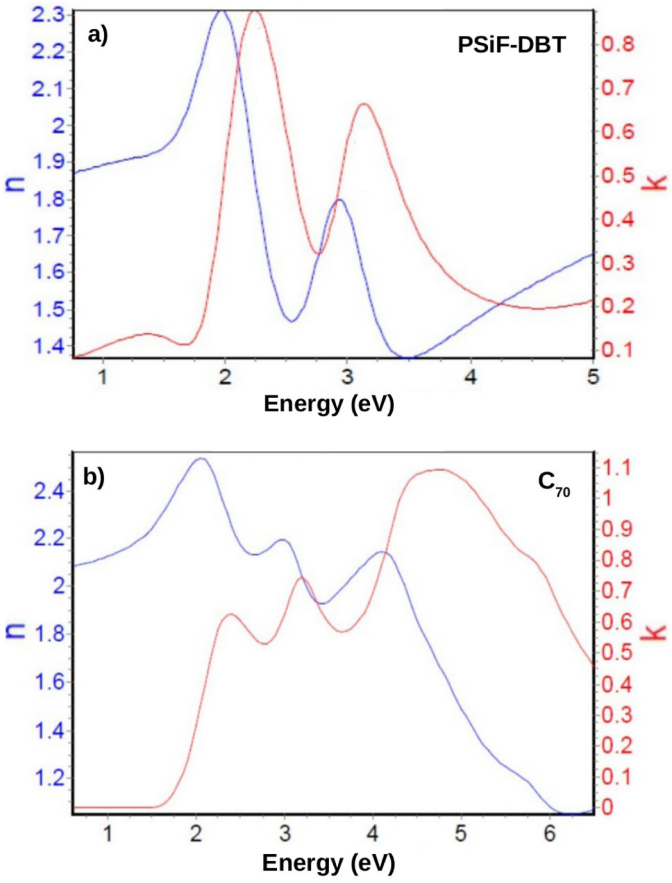

Fig. 2. – Optical parameters of (a) PSiF-DBT and (b) C_{70}.

2.2. Optical modeling and computational methods

We carried out numerical simulation to calculate absorption of multilayer structures following the transfer matrix method [34–36] which assumes a perfect bilayer with a sharp interface and depends on the optical constants of the materials. The C_{60} and PEDOT-PSS optical constants were taken from [34,37] whereas the optical constants for the ITO and Al layers were obtained from Ref [38]. The optical constants of the PSiF-DBT and C_{70} layers were determined by variable angle spectroscopic using a Horiba UVISEL 2 Spectroscopic Phase Modulated Ellipsometer (Fig. 2). Following the transfer matrix method, we obtain the contribution of each layer in the absorption of the device. Using the one-dimensional exciton diffusion equation, we also obtained the theoretical External Quantum Efficiency (EQE) considering that the photocurrent is formed by the excitons that dissociate near the PSiF-DBT/fullerene and fullerene/Al interfaces. The theoretical EQE curve is fitted to the experimental result by varying the diffusion length of the excitons (L) in the polymer and fullerene layers. This fitting is used to evaluate the degree of polymer/fullerene intermixing at the interface of the bilayer device [32] .

In relation to the quantum chemical calculations, the fullerene molecules and the model clusters were simulated as follows: first the structure of the isolated fullerenes was fully optimized using Hartree-Fock (HF) method and the 3–21G** basis set. After this previous geometry optimization the cluster were built, containing 4 and 8 fullerene molecules, and submitted to a molecular dynamics (MD) simulation using Andersen thermostat [39] and van der Waals dispersion correction[40], as implemented in density functional-based tight binding code [41] . Electronic transitions were obtained using the Zerner's Intermediate Neglect of Differential Overlap (ZINDO) semi-empirical method as implemented in the ORCA package [42] . The same procedures were used to calculate the electronic transition for a model structure (containing 5 repeated units) of the PSiF-DBT copolymer.

Noncovalent interactions between two fullerene molecules were analyzed using density functional theory (DFT) with the dispersion corrected wB97XD [43] functional and 6–31G* basis set [44,45] as implemented in the Gaussian 09 package [46] . The distance between the molecules (with the frozen geometry derived from HF/3–21G** optimization step described above) was varied to calculate the interaction energy profile as a function of the separation distance between the fullerenes. Those calculations were performed assuming different relative orientations of the two fullerene molecules in the complex.

3. Results and discussion

In this section we briefly revise relevant characteristics of the PSiF-DBT and $C_{60(70)}$ layers. As well as show and discuss some results that further stress the key differences between the C_{60} and C_{70} fullerene films. Those discussions (together with optical modeling assuming ideal bilayer devices) will base our understanding of the main phenomena that affects the photovoltaic characteristics of the PSiF-DBT/$C_{60(70)}$ devices.

3.1. The PSiF-DBT layer

In a previous work, we reported the main electronic transitions that

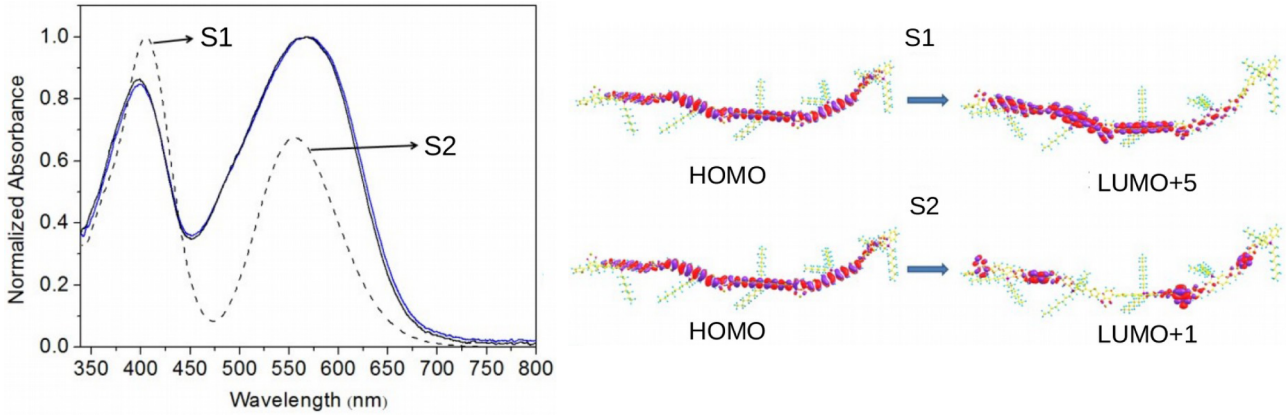

Fig. 3. – UV–Vis spectra for PSiF-DBT thin film as cast (black line) and annealed at 100 °C (blue line). Dashed line shows the simulated absorption spectrum of a model oligomer of PSiF-DBT containing 5 units. This result was obtained using the ZINDO approximation as implemented in ORCA package. In the left we show the principal molecular orbital contributing to S1 and S2 absorption bands. (For interpretation of the references to color in this figure legend, the reader is referred to the web version of this article.)

contribute for the absorption spectrum of the PSiF-DBT which is showed in Fig. 3 [47] . The absorption band at 390 nm (3.18 eV) band has a strong π-π* character and mainly corresponds to electronic transitions involving orbitals which are delocalized along the PSiF-DBT. On the other hand, the absorption band at 560 nm (2.21 eV) has an internal charge transfer (ICT) characteristic since this electronic transition involves unoccupied molecular orbitals centered around the benzothiadiazole group (internal acceptor group) and occupied molecular orbitals more delocalized over backbone of the polymer (see Fig. 3). The strong ICT character of this lower-energy absorption band (that has a higher overlap with the solar spectrum) may contribute to efficient exciton dissociation since this kind of transition produces a longer intrachain separation between the photoexcited electron-hole pair [7,48–50] . Those properties thus indicate that the PSiF-DBT is indeed a very promising material for photovoltaic applications.

Another key-point to understand the photovoltaic properties of our devices is that the PSiF-DBT is able to form very packed thin films even without any thermal annealing treatment. Using the Positron Annihilation Spectroscopy (PAS) technique, [51] we showed recently that the material packing does not change even when the PSIF-DBT films are submitted to annealing at temperatures up to 200 °C. As a consequence, the thermal annealing is able to induce only a modest rise of the effective hole mobility in the PSIF-DBT film. This behavior was in contrast to what is observed in a similar donor-acceptor copolymer in which the hole mobility increases by several orders of magnitude after the thermal treatment [8] . However, an improvement in J_{SC} of photovoltaic devices (and consequently in PCE) was achieved when the PSiF-DBT layer was submitted to the annealing process prior to the acceptor deposition. This effect was attributed to the roughness increase of the polymeric surface which (i) provides an enhanced donor/acceptor contact area and (ii) assists the fullerene diffusion creating an mixed layer close to the so called bulk heterojunction [51] . The surface roughness enhancement after annealing will be revisited here to discuss the effects originated from different diffusivities of the C_{60} and C_{70} into the polymeric layer.

3.2. The C_{60} and C_{70} layers

As a result of the distinct symmetries, the electronic, vibrational and dynamic properties of the two fullerenes are quite different. For instance, C_{60} has a low absorption coefficient in the visible range of light exhibiting a weak contribution to the generated photocurrent in photovoltaic devices. On the other hand, C_{70} has a stronger absorption in this spectral range, leading to a higher exciton generation and consequently an increase of photocurrent. This effect happens despite both fullerenes have approximately the same optical bandgap (around 1.76 eV). The explanation resides in the lower symmetry of the C_{70} that lifts the degeneracy of many electronic transitions in the absorption spectrum of the C_{60} [52] . Moreover, electronic transitions with low energy derived from the HOMO→LUMO excitations are symmetry forbidden in the C_{60} because they involve states with the same parity (h_u for HOMO orbital and t_{1u} for LUMO orbital) [52] . In contrast, the symmetries of the two HOMOs and the two LUMOs of the C_{70} give rise to dipole allowed low energy excited states. Hence this molecule has a higher number of dipole-allowed transitions in the visible range when compared to the C_{60}. Those features are clear in Fig. 4 where we compared the measured absorption spectra of both fullerenes films to the calculated vertical electronic transitions of isolated molecules. As we show in Fig. 4, there are many electronic vertical transitions in the C_{70} molecule that are not observed in the C_{60} molecule. One can also see that the transitions calculated for the isolated fullerenes do not correspond to many structures of the measured spectra for wavelengths longer than 400 nm in C_{60} and 600 nm in C_{70}. Those structures are derived from intermolecular interactions on the electronic transitions of the isolated molecule.

The molecule shape significantly interferes on the electronic structure of the fullerenes. The additional belt of planar hexagonal rings around the C_{70} equator increases the π-character of this molecule when compared to the spherical C_{60}. This effect may increase the electronic coupling among aggregates of C_{70} molecules. The optical properties of the C_{60} and C_{70} films measured by Kazaoui et al. [20] using several spectroscopic measurements are in agreement with this hypothesis. They showed that the 0–0 electronic transitions corresponding to Frenkel excitons (intramolecular electronic transitions) are observed at energies with approximated values in both fullerenes. Yet the CT excitons are observed at lower energies in C_{70} compared to the C_{60}. The lower excitation energy necessary to create a CT exciton in C_{70} indicates that the intermolecular electronic couplings are higher in this kind of fullerene. This property favors electronic transport which results in lower R_s in photovoltaic devices using C_{70}.

An indication of this effect is found in Fig. 5 that shows the absorption spectrum of C_{60} and C_{70} films for wavelengths above 400 nm. In this figure, it is also included the vertical electronic transitions of model clusters of C_{60} and C_{70} molecules calculated using the semi-empirical ZINDO approximation. The structures of those aggregates are shown in the up-right corner of the respective figure. The electronic transitions calculated for a cluster composed by four C_{60} molecules is enough to reproduce the main features of the C_{60} film spectra at longer wavelengths. Nevertheless, it is necessary a cluster of at least eight molecules to reproduce the absorption features of the C_{70} film in the same range of wavelengths. The bestnumber of coupled molecules to reproduce the experimental result were found performing a systematic study where we compared the theoretical transitions for a growing number of C_{60} and C_{70} aggregates with the respective experimental absorption spectrum. For simplicity we did not showthose results here. We point out that thiscomparison was not made to estimate the cluster size of the molecules, but rather to verify the number of electronic coupled C_{70} and C_{60} molecules in each aggregate, as mentioned in the discussion of the previous paragraph.

In order to verify if indeed the intermolecular interactions are stronger for the C_{70} molecules, we computed the potential energy curve (PEC) between two $C_{60(70)}$ molecules at the DFT/WB97XD/6–31 g* level of theory. The distance (*d*) between two fullerenes was varied in 0.1 Å steps to construct the interaction profile assuming three different relative orientations of the fullerene molecules. Those orientations are illustrated in Fig. 6a. For the C_{70} complex they are built so that (i) one hexagonal ring at the equator of the first molecule is facing one hexagonal ring at the equator of other molecule (HE−HE complex); (ii) one hexagonal ring at the equator of the first molecule faces a pentagonal ring at the pole of the other molecule (HE−PP complex) or (iii) when the pentagonal ring at the pole of the first molecule is facing the pentagonal ring at the pole of the other fullerene (PP−PP complex). By the same token, we calculated the PEC for the C_{60} dimers when the (i) one hexagonal ring of the first fullerene faces the equivalent ring of the other fullerene (H−H complex); (ii) one hexagonal ring of the first molecule faces one pentagonal ring of the second fullerene (H−P complex) or (iii) one pentagonal ring of the first C_{60} faces the equivalent ring of other fullerene (P−P complex).

The depths of the potential wells in Fig. 6b are around 0.35 eV which is general agreement with symmetry-adapted perturbation theory calculation performed for C_{60} molecules [53] . Yet potential depths between two C_{70} molecules tend to be higher compared to the C_{60} complex with the equivalent orientation. For instance, the C_{70}−C_{70} interaction in the HE-HE orientation is approximately 0.05 eV more stable than the C_{60}−C_{60} interaction in the H−H orientation. Once the C_{70} fullerene has five more hexagonal sp^2 rings at the equator than does the C_{60} molecule, the surface of C_{70} is more graphitic like than that of C_{60}. As expected, this property increases the π-π interaction between the C_{70} fullerenes in the HE−HE orientation.

The variations in the equilibrium distance (the position of the PEC's minimum) between the fullerene molecules are mainly determined by differences in the exponential increase of the PEC at small distances.

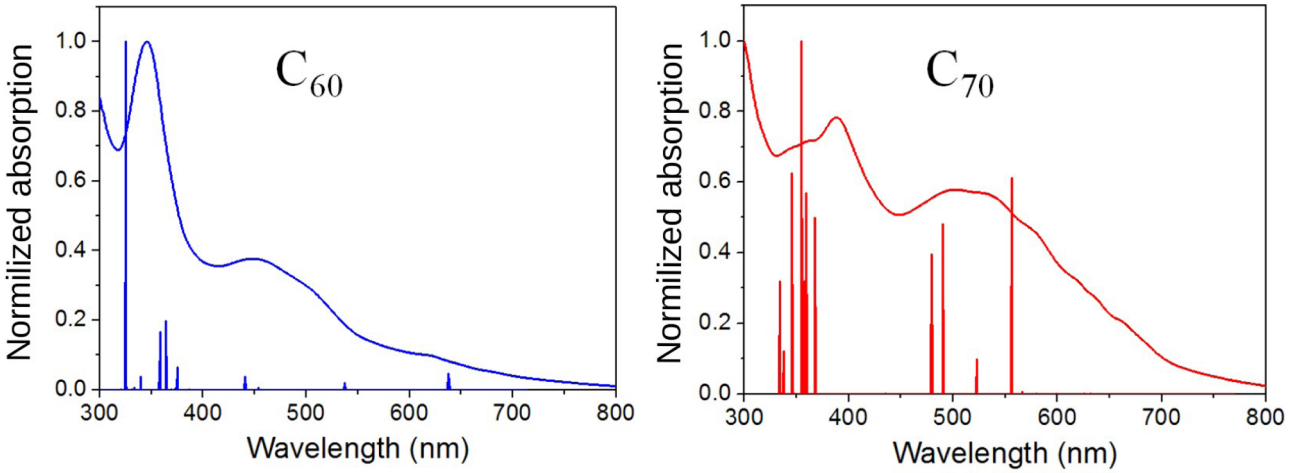

Fig. 4. – Absorption spectra of C_{60} and C_{70}. The vertical lines show the simulated vertical electronic transitions of C_{60} and C_{70} isolated molecules. All simulations were performed using the semi-empirical ZINDO approximation as implemented in ORCA package.

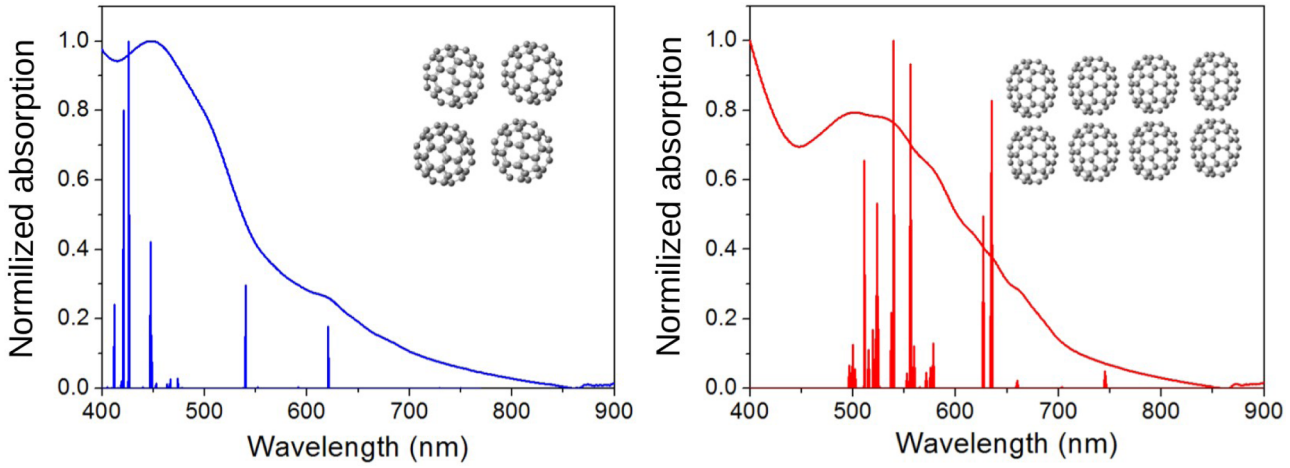

Fig. 5. – The absorption spectra of C_{60} (left) and C_{70} (right) films (continuous lines) and the simulated vertical electronic transitions of C_{60} and C_{70} model clusters. The final morphology of C_{60} (left) and C_{70} (right) clusters (obtained using MD simulations, see the text) are illustrated at the top right corner of the respective picture. Electronic transitions were calculated using the semi-empirical ZINDO approximation as implemented in ORCA package.

This part of the PEC is related to the exchange-repulsion energy when there is a significant overlap of occupied orbitals between the two molecules [53] . The increase of the PEC happens then at smaller distances when the electron-deficient pentagonal rings of each molecule are interacting more directly (P—P orientation). This effect also explains why the exponential rise of the PEC for the C_{60} happens at longer distances than that of C_{70}: the degeneracy of the occupied frontier orbitals due to the higher symmetry of the C_{60} fullerene enhances the exchange repulsion. Hence (with the exception of the C_{60} P—P complex) this repulsive part of the PEC tends to rise at smaller distances for the complexes with C_{70} which indicates not only a tighter packing but also a closer packing for C_{70} the aggregates.

These results are further supported by X-ray diffraction measurements of the fullerene films. Rietveld refinement was performed for the [111] reflection [54]; this particular peak was selected because it appears at a low value of 2θ and should thus be the most unaffected by any broadening induced by the geometry of the measurement (see Fig. 7a)). The experimental resolution was modeled with an angular dependence of the peak width according to Caglioti's formula. We extracted the crystallite size according to Scherrer's formula simplified for cubic symmetry: $\Delta(2\theta) = \lambda/L \cdot \cos(\theta)$, where $\Delta(2\theta)$ is the crystallinity-related broadening, λ the wavelength and L the size of the average crystalline region [54] . The peak profile presents a low-2θ shoulder, which is commonly observed in fullerenes and is due to stacking faults that are not indexed by the Fm-3 m symmetry [55] . We considered thus the high-2θ region of the peaks only and the results of the refinements indicate crystallite sizes of 16.9 and 18.7 nm for C_{60} and C_{70}, respectively. AFM topography images, Figs. 6b and 6c, indicate that indeed C_{70} tends to form bigger crystalline domains than the domains of C_{60} molecules.

3.3. *PSiF-DBT/$C_{60(70)}$ organic photovoltaic devices*

We will now analyze the photovoltaic response of the devices using PSiF-DBT as donor and C_{60} or C_{70} as acceptor. Fig. 8a shows the $J \times V$ characteristics under illumination of 100 mW/cm^2 for PSiF-DBT/C_{60} and PSiF-DBT/C_{70} devices whereas the polymeric layer was annealed at 100 °C. The photovoltaic parameters of these devices are summarized in Table 1. It is clear that the devices based on C_{70} have better performance when compared to the respective devices based on C_{60}. There is an increase in J_{SC} when C_{70} is the electron acceptor which agrees with previous works that compared the performances of these fullerenes in small-molecules based solar cells [56–58] . The improved performances of the devices containing C_{70} are attributed to the higher absorption coefficient of this fullerene in the visible range. For instance, an elementary optical analysis using the transfer matrix method [34] and assuming a sharp transition between the polymer and the fullerene layers agrees with this hypothesis as shown in Fig. 9. It also indicates

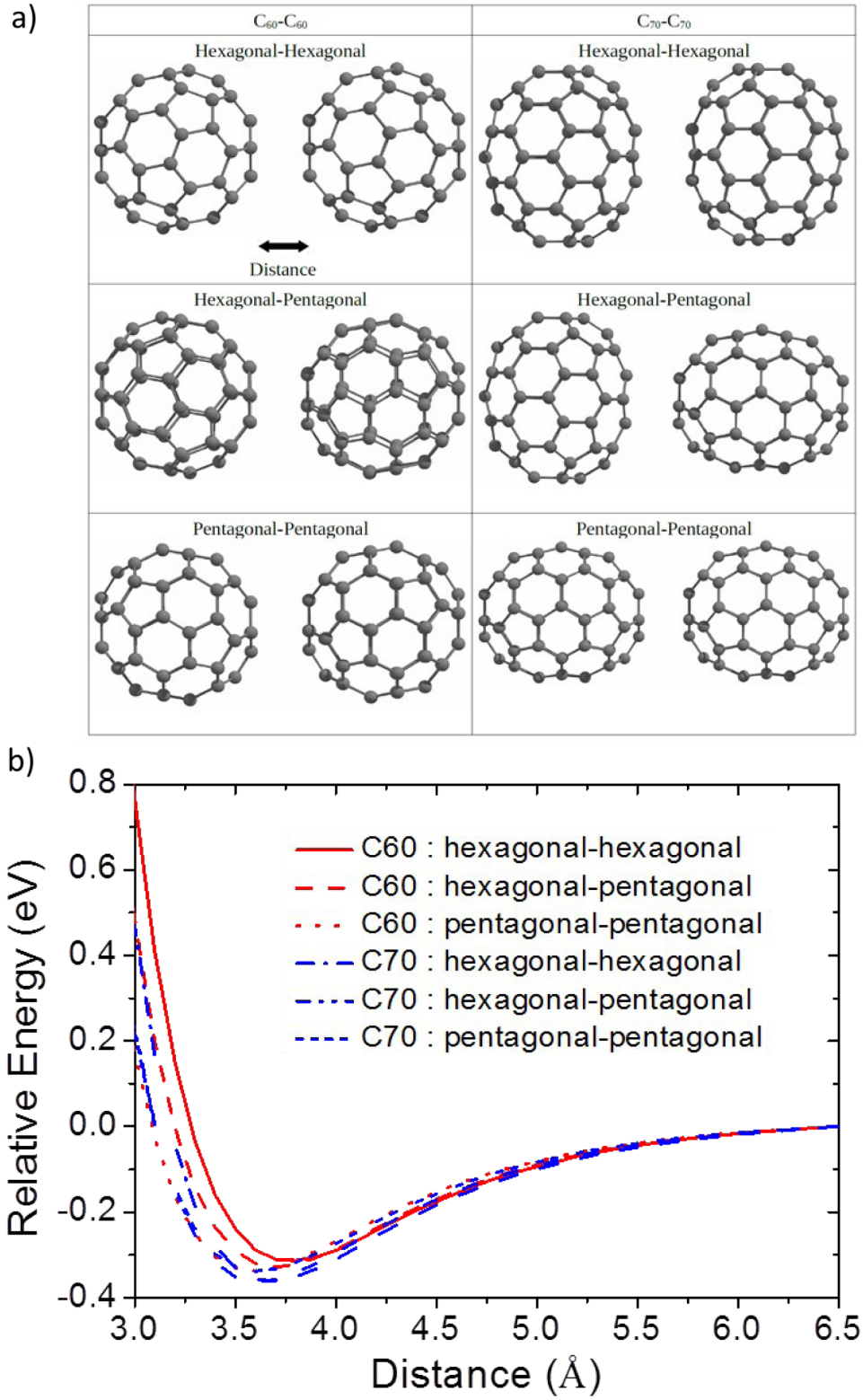

Fig. 6. - (a) The three orientations for the C_{60} (left) and C_{70} molecules (right) in the dimers employed to calculate the respective (b) interaction energy curve for different distances between the fullerenes molecules. The curves in Fig. 6(b) were calculated at DFT/WB97XD/6–31G* level of theory.

that the C_{70} device would absorb a higher fraction of light in the wavelengths between 525 and 650 nm than the respective C_{60} device with the same thicknesses of the multilayered structure. It follows then that the device with C_{70} reflects a lower fraction of the incident radiation which improves the photons harvesting in the visible range. The key role played by the C_{70} optical properties is also supported by the External Quantum Efficiency (EQE) of the PSiF-DBT/C_{60} and PSiF-DBT/C_{70} devices (see Fig. 8). One can see that around 550–600 nm the photocurrent generation is mainly dominated by the absorption properties of the copolymer in both kind of devices. Nevertheless, the device with C_{70} has a broad activity in visible range of the spectrum with additional contributions to the EQE in the interval between 600 and

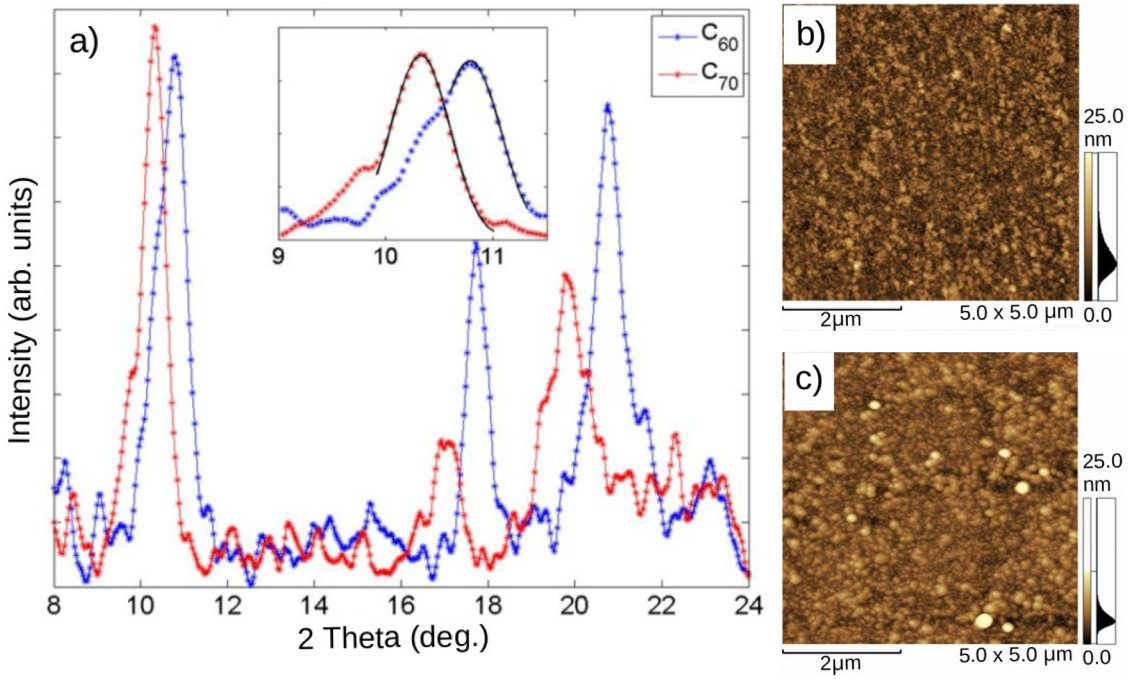

Fig. 7. – (a) X-ray diffraction measurements of the fullerene films (Rietveld refinement was performed for the [111] reflection). AFM topography images of b) C_{60} and c) C_{70}.

700 nm. This result is in trend with the absorption profiles of both PSiF-DBT and C_{70} (see Fig. 8b dashed line and inset). C_{70} presents a higher absorption than the C_{60} in the range that corresponds to the wavelengths between the main absorption bands of PSiF-DBT. As consequence, the EQE of the C_{70} based device exhibits a flatter plateau in the vicinities of the 50% efficiency for a wider range of light frequencies.

Furthermore, the comparison between the ZINDO simulations and the experimental spectra of the C_{70} film showed in Fig. 5 indicates that a significant contribution to light absorption above 525 nm comes from the excitonic splitting of the single molecule transitions induced by molecular aggregation. Hence the capacity of the C_{70} to form larger molecular aggregates is a characteristic that improves its photovoltaic properties by producing broad photon absorption along the visible range of the solar spectrum.

The annealed devices based on C_{60} as acceptor have a J_{SC} of 10.64 mA/cm^2, open circuit voltage (V_{OC}) of 0.79 V and fill factor (FF) of 47% resulting in a PCE of 3.99%. The annealed devices based on C_{70} have a J_{SC} of 16.85 mA/cm^2 and V_{OC} of 0.72 V with FF of 47% resulting in a PCE of 5.75%. The improvement of solar cell performance after the thermal treatment at 100 °C is more pronounced for the device using the lighter fullerene (see Table I). The reasons behind this effect are not clear. For instance, J_{SC} increases by 92% for the device with C_{60} upon annealing. On the other hand, the increase of J_{SC} is considerably lower for the device with C_{70} (62%). The rise of J_{SC} upon annealing can be attributed to the increase in the PSiF-DBT film's roughness [51] . The easier diffusion of the acceptor into the polymeric film increases then the donor/acceptor (D/A) contact area for exciton dissociation. Since the C_{60} aggregates are smaller than C_{70} aggregates, C_{60} has a greater capacity to penetrate into (the thermally treated) polymeric film during the evaporation process. The increase of the J_{SC} induced by the thermal treatment is then higher for the PSiF-DBT/C_{60} solar cells.

The EQE measurements in combination with optical modeling give support to this interpretation. As proposed in Ref. [32], this method can be used as an indicator of the bilayer interfacial mixing. In Fig. 10, we show that theoretical EQE calculated using the optical field distribution for a sharp polymer/fullerene interface and the one-dimensional exciton diffusion is not able to successfully reproduce the profile of the experimental EQE measured in PSiF-DBT/C_{60} device treated at 100 °C (even if one assumes an unrealistic value for exciton diffusion length around the same order of the thickness of the fullerene layer, L_{C60} = 34 nm). The thermal treatment assists the C_{60} diffusion into the polymeric layer so those device does not behave as a bilayer one. On the other hand, using exciton diffusion lengths in agreement with values in the literature (L_{C70} = 17 nm) [59], theoretical EQE follows closely the experimental EQE of PSiF-DBT/C_{70} devices. This result indicates that the C_{70} devices preserve their bilayer-like morphology due to the smaller depth of C_{70} penetration induced by the thermal annealing. This is consistent with the hypothesis that the C_{70} aggregates are bigger than the C_{60} aggregates which considerably reduces their diffusion in the polymeric layer during the deposition process.

In Table 1 one can also see that there is a small increase of V_{OC} in C_{60} devices in contrast to a loss of V_{OC} in the C_{70}-based devices after the thermal treatment. Those results confirm that the thermal treatment is more effective to improve the photovoltaic performance of the devices based on C_{60}. As a result, the PCE of the C_{60} solar cells almost double whereas the PCE of the C_{70} devices increases only by a 1.69 factor with the annealing process. This result gives further support to the idea that the lower sizes of the C_{60} aggregates produce a deeper penetration of these molecules inside the annealed polymeric film. Yet the solar cells using the C_{70} still have a higher PCE (as for the as cast devices) mainly due to its improved optical absorption in the long wavelength range of the solar spectrum.

The gain of performance observed in the C_{70} is not produced only by the superior optical properties of this fullerene. Improved transport properties of the C_{70} film play an important role as well.

It is known that the charge transport in organic solar cells is unbalanced due to the higher magnitude of the hole mobility compared to the magnitude of the electron mobility in the fullerene layer. This unbalanced charge transport tends to increase the R_s of the devices. It can be seen in Table 1 that the C_{70} devices always have a lower R_s than does the C_{60} devices. Since the acceptor layer evaporated in both kind of solar cells have approximately the same thickness, this indicates that the charge transport is probably more balanced when the C_{70} is used as acceptor. A closer look to the PEC's of Fig. 6b helps to explain this effect. In this Figure it is clear that the equilibrium distances between

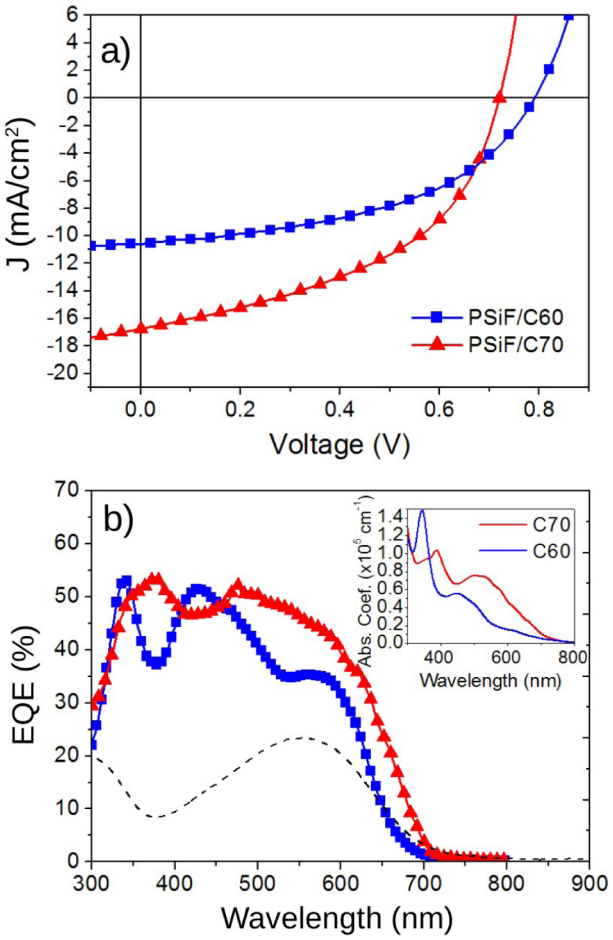

Fig. 8. – (a) *J-V* characteristic for ITO/PEDOT:PSS/PSiF-DBT/C_{60}/Al and ITO/PEDOT:PSS/PSiF-DBT/C_{70}/Al device annealed at 100 °C. (b) EQE for the same PSiF/C_{60} and for the PSiF/C_{70} devices and UV–Vis spectrum of a PSiF-DBT thin film (dashed line). Inset Figure shows the absorption coefficient of C_{60} (dashed black line) and C_{70} (black line).

fullerene dimers tend to be slightly smaller for C_{70} molecules. As a consequence, the better overlap of the molecular orbitals favors the electronic transport in C_{70} which partially compensates the higher hole mobility along the polymeric layer. The improvement of the electronic overlap is also one possible reason behind the strong reduction of the R_s for C_{70} devices submitted to thermal annealing. In those samples, R_S drops by 1/3 which compensates the simultaneous reduction of the shunt resistance (R_{sh}) (that drops by 1/2). This result is in agreement with measurements that found higher electrical conductivity values for the C_{70} film compared to C_{60} film both in dark and under illumination [58] . As a result of the improved charge carrier transport, the fill factor of the C_{70} samples submitted to the annealing process is higher than the FF of as cast devices.

5. Conclusions

We have studied the photovoltaic properties of devices using PSiF-DBT as donor layer and C_{60} or C_{70} as acceptor layer. The C_{70} based devices showed a superior photovoltaic performance compared to the C_{60} devices with and without thermal annealing treatment of the polymeric layer. We highlight two crucial points to explain those results: (i) C_{70} is able to absorb a bigger portion of the incoming photons from the solar spectrum. (ii) The improved π-π character of the C_{70} increases the inter-chain coupling between molecules that enhancing the charge carrier transport along the acceptor layer which results in lower R_s of the devices. Despite the better performance of the C_{70} based devices, after the annealing treatment at 100 °C, the increase of J_{SC} is approximately twice greater when the C_{60} is the acceptor. This happens because morphological changes of the PSiF-DBT film surface after annealing might facilitate the penetration of C_{60} aggregates inside the polymer layer leading to a better mix between donor and acceptor species. Therefore, from the comparison of photovoltaic devices using C_{60} or C_{70} as acceptor, it is clear that the use of an acceptor with a complementary absorption profile to the polymer's absorption spectrum can significantly improve the spectral response of photovoltaic devices. This match of optical properties of the donor and the acceptor species together with a better control of the size of the fullerene aggregates relative to the roughness of the polymeric layer may be a promising approach to further enhance the efficiency of fullerene-based solar cells.

CRediT authorship contribution statement

L. Benatto: Writing - original draft, Visualization, Investigation, Software. **C.F.N. Marchiori:** Writing - review & editing, Conceptualization, Investigation, Software. **T. Talka:** Investigation, Validation. **M. Aramini:** Investigation, Validation. **N.A.D. Yamamoto:** Investigation, Validation. **S. Huotari:** Supervision, Investigation, Formal analysis. **L.S. Roman:** Supervision, Resources, Writing - review & editing. **M. Koehler:** Supervision, Writing - review & editing, Project administration.

Declaration of Competing interest

The authors declare that they have no known competing financial interests or personal relationships that could have appeared to influence the work reported in this paper.

Acknowledgments

This work has been supported by the Companhia Paranaense de Energia – COPEL research and technological development program, through the PD 2866-0470/2017 project, regulated by ANEEL. This study was financed in part by the Coordenação de Aperfeiçoamento de Pessoal de Nível Superior-Brasil (CAPES)-Finance Code 001. The research was developed with the assistance of CENAPAD-SP (Centro Nacional de Processamento de Alto Desempenho em São Paulo), project UNICAMP/FINEP-MCT. Special thanks go to CNPq (grant 380163/2019-5) and INCT Nanocarbon for the financial support. Tuomas Talka, Matteo Aramini and Simo Huotari were supported by Academy of Finland (grant 1295696). Special thanks go to Horiba for their courtesy with the measurements of optical constants.

Table 1
– Photovoltaic parameters measured in the C70 and C60 devices as cast and after annealing at 100 °C.

Device		V_{oc}(V)	J_{sc}(mA/cm^2)	R_s(Ω.cm^2)	R_{sh}(Ω cm^2)	FF(%)	PCE(%)
PSiF-DBT/C_{60}	As cast	0.77	5.55	30.25	446.77	47	2.00
	100 °C	0.79	10.64	15.23	241.23	47	3.99
PSiF-DBT/C_{70}	As cast	0.76	10.37	21.82	203.97	43	3.40
	100 °C	0.72	16.85	6.87	116.82	47	5.75

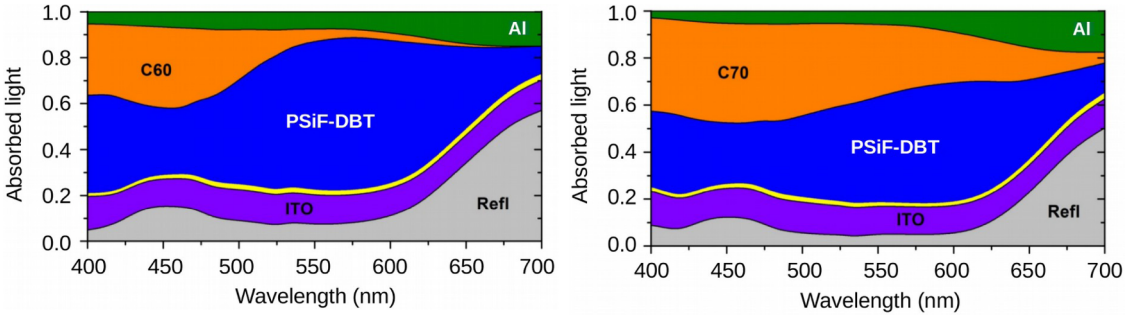

Fig. 9. - Calculated fraction of absorbed radiation in each layer and the total reflection in an ideal bilayer device with glass (1 mm)/ITO (120 nm)/PEDOT-PSS (40 nm)/PSiF-DBT (22 nm)/C_{60} or C_{70} (34 nm)/Al (70 nm) as calculated using the transfer matrix method. The thin yellow stripes correspond to the fraction of light absorbed in the PEDOT-PSS layer. (For interpretation of the references to color in this figure legend, the reader is referred to the web version of this article.)

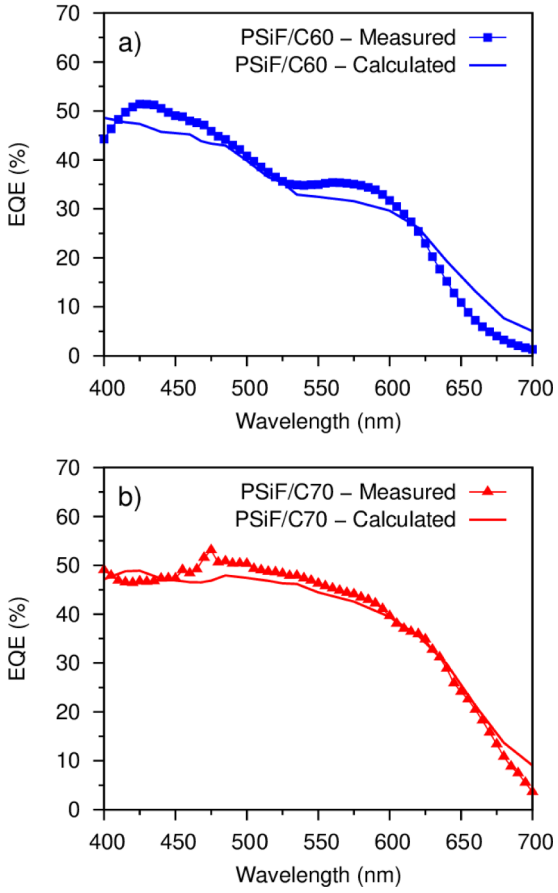

Fig. 10. – Measured and calculated EQE for (a) ITO/PEDOT:PSS/PSiF-DBT/C_{60}/Al and (b) ITO/PEDOT:PSS/PSiF-DBT/C_{70}/Al devices annealed at 100 °C. The calculated EQE was obtained using the transfer matrix method and the one-dimensional exciton diffusion equation. We assume that the excitons are quenched at PSiF-DBT/$C_{60(70)}$ interface and at the $C_{60(70)}$/Al interface. The continuous curves were calculated using the exciton diffusion length (L) at the polymer and fullerene layers as adjustment parameters. The best theoretical fit of the experimental EQE were obtained for (a) with L_p = 18 nm and L_{C60} = 34 nm and for (b) with L_p = 11 nm and L_{C70} = 17 nm.

References

[1] H. Hoppe, N.S. Sariciftci, Organic solar cells: an overview, J. Mater. Res. 19 (2004) 1924–1945, https://doi.org/10.1557/JMR.2004.0252.

[2] R.R. Søndergaard, M. Hösel, F.C. Krebs, Roll-to-roll fabrication of large area functional organic materials, J. Polym. Sci. Part B Polym. Phys. 51 (2013) 16–34, https://doi.org/10.1002/polb.23192.

[3] R. Søndergaard, M. Hösel, D. Angmo, T.T. Larsen-Olsen, F.C. Krebs, Roll-to-roll fabrication of polymer solar cells, Mater. Today 15 (2012) 36–49, https://doi.org/10.1016/S1369-7021(12)70019-6.

[4] T.R. Andersen, H.F. Dam, M. Hösel, M. Helgesen, J.E. Carlé, T.T. Larsen-Olsen, S.A. Gevorgyan, J.W. Andreasen, J. Adams, N. Li, F. Machui, G.D. Spyropoulos, T. Ameri, N. Lemaître, M. Legros, A. Scheel, D. Gaiser, K. Kreul, S. Berny, O.R. Lozman, S. Nordman, M. Välimäki, M. Vilkman, R.R. Søndergaard, M. Jørgensen, C.J. Brabec, F.C. Krebs, Scalable, ambient atmosphere roll-to-roll manufacture of encapsulated large area, flexible organic tandem solar cell modules, Energy Environ. Sci. 7 (2014) 2925–2933, https://doi.org/10.1039/c4ee01223b.

[5] D.M. Stoltzfus, J.E. Donaghey, A. Armin, P.E. Shaw, P.L. Burn, P. Meredith, Charge generation pathways in organic solar cells: assessing the contribution from the electron acceptor, Chem. Rev. 116 (2016) 12920–12955, https://doi.org/10.1021/acs.chemrev.6b00126.

[6] M. Koehler, L.S. Roman, O. Inganäs, M.G.E. Da Luz, Modeling bilayer polymer/fullerene photovoltaic devices, J. Appl. Phys. 96 (2004) 40–43, https://doi.org/10.1063/1.1759786.

[7] C.D. Canestraro, P.C. Rodrigues, C.F.N. Marchiori, C.B. Schneider, L. Akcelrud, M. Koehler, L.S. Roman, The role of the double peaked absorption spectrum in the efficiency of solar cells based on donor-acceptor-donor copolymers, Sol. Energy Mater. Sol. Cells 95 (2011) 2287–2294, https://doi.org/10.1016/j.solmat.2011.03.043.

[8] A.G. Macedo, C.F.N. Marchiori, I.R. Grova, L. Akcelrud, M. Koehler, L.S. Roman, Hole mobility effect in the efficiency of bilayer heterojunction polymer/C60 photovoltaic cells, Appl. Phys. Lett. 98 (2011) 98–101, https://doi.org/10.1063/1.3601476.

[9] C.F.N. Marchiori, N.A.D. Yamamoto, I.R. Grova, A.G. MacEdo, M. Paulus, C. Sternemann, S. Huotari, L. Akcelrud, L.S. Roman, M. Koehler, Performance of fluorene and terthiophene copolymer in bilayer photovoltaic devices: the role of the polymer conformations, Org. Electron. Phys. Mater. Appl. 13 (2012) 2716–2726, https://doi.org/10.1016/j.orgel.2012.08.002.

[10] O.D. Lourenco, L. Benatto, C.F.N. Marchiori, H.C. Avila, N.A.D. Yamamoto, C.K. Oliveira, M.G.E. Da Luz, M. Cremona, M. Koehler, L.S. Roman, Conformational change on a bithiophene-based copolymer induced by additive treatment: application in organic photovoltaics, J. Phys. Chem. C. 121 (2017) 16035–16044, https://doi.org/10.1021/acs.jpcc.7b05427.

[11] M. Koehler, M.C. Santos, M.G.E. Da Luz, Positional disorder enhancement of exciton dissociation at donor/acceptor interface, J. Appl. Phys. (2006) 99, https://doi.org/10.1063/1.2174118.

[12] P.C. Eklund, A.M. Rao, Y. Wang, P. Zhou, K.A. Wang, J.M. Holden, M.S. Dresselhaus, G. Dresselhaus, Optical properties of C60- and C70-based solid films, Thin Solid Films 257 (1995) 211–232, https://doi.org/10.1016/0040-6090(94)05706-0.

[13] H.W. Kroto, J.R. Heath, S.C. O'Brien, R.F. Curl, R.E. Smalley, C60: buckminsterfullerene, Nature 318 (1985) 162–163, https://doi.org/10.1038/318162a0.

[14] J. Hare, H. Kroto, R. Taylor, Preparation and UV/visible spectra of fullernes C60 and C70, Chem. Phys. Lett. 177 (1991) 394–398, https://doi.org/10.1016/j.cplett.2013.08.068.

[15] F. Wudl, N. Sariciftci, L. Smilowitz, A.J. Heeger, Photoinduced electron transfer from a conducting polymer to buckminsterfullerene, Science (80-) 258 (1992) 1474–1476, https://doi.org/10.1080/00472338380000161.

[16] B. Kraabel, C.H. Lee, D. Mcbranch, D. Moses, N.S. Sariciftci, A.J. Heeger, Ultrafast photoinduced electron transfer in conducting polymer-buckminsterfullerene composites, Chem. Phys. Lett. 213 (1993) 389–394, https://doi.org/10.1016/0009-2614(93)85151-D.

[17] B. Kraabel, D. McBranch, N.S. Sariciftci, D. Moses, A.J. Heeger, Ultrafast spectroscopic studies of photoinduced electron transfer from semiconducting polymers to C60, Phys. Rev. B 50 (1994) 18543–18552, https://doi.org/10.1103/PhysRevB.50.18543.

[18] N.S. Sariciftci, Role of buckminsterfullerene, C60, in organic photoelectric devices, Prog. Quantum. Electron. 19 (1995) 131–159, https://doi.org/10.1016/0079-6727(94)00012-N.

[19] A. Graja, J.P. Farges, Optical spectra of C60 and C70 complexes: Their similarities and differences, Adv. Mater. Opt. Electron. 8 (1998) 215–228. 10.1002/(SICI)1099-0712(1998090)8:5<215::AID-AMO338>3.0.CO;2-%23.

[20] S. Kazaoui, N. Minami, Intermolecular charge transfer excitons in C70 as compared with C60 films, Synth. Met. 86 (1997) 2345–2346, https://doi.org/10.1016/S0379-6779(97)81154-X.

[21] H. Zhou, L. Yang, W. You, Rational design of high performance conjugated polymers for organic solar cells, Macromolecules 45 (2012) 607–632, https://doi.org/10.1021/ma201648t.
[22] E. Wang, L. Wang, L. Lan, C. Luo, W. Zhuang, J. Peng, Y. Cao, High-performance polymer heterojunction solar cells of a polysilafluorene derivative, Appl. Phys. Lett. 92 (2008) 2–5, https://doi.org/10.1063/1.2836266.
[23] M.C. Scharber, M. Koppe, J. Gao, F. Cordella, M.A. Loi, P. Denk, M. Morana, H.J. Egelhaaf, K. Forberich, G. Dennler, R. Gaudiana, D. Waller, Z. Zhu, X. Shi, C.J. Brabec, Influence of the bridging atom on the performance ofa low-bandgap bulk heterojunction solar cell, Adv. Mater 22 (2010) 367–370, https://doi.org/10.1002/adma.200900529.
[24] H.Y. Chen, J. Hou, A.E. Hayden, H. Yang, K.N. Houk, Y. Yang, Silicon atom substitution enhances interchain packing in a thiophene-based polymer system, Adv. Mater. 22 (2010) 371–375, https://doi.org/10.1002/adma.200902469.
[25] M. Morana, H. Azimi, G. Dennler, H.J. Egelhaaf, M. Scharber, K. Forberich, J. Hauch, R. Gaudiana, D. Waller, Z. Zhu, K. Hingerl, S.S. Van Bavel, J. Loos, C.J. Brabec, Nanomorphology and charge generation in bulk heterojunctions based on low-bandgap dithiophene polymers with different bridging atoms, Adv. Funct. Mater. 20 (2010) 1180–1188, https://doi.org/10.1002/adfm.200900931.
[26] M. Arar, A. Pein, W. Haas, F. Hofer, K. Norrman, F.C. Krebs, T. Rath, G. Trimmel, Comprehensive investigation of silver nanoparticle/aluminum electrodes for copper indium sulfide/polymer hybrid solar cells, J. Phys. Chem. C. 116 (2012) 19191–19196, https://doi.org/10.1021/jp306242e.
[27] M. Jäger, R. Trattnig, M. Postl, W. Haas, B. Kunert, R. Resel, F. Hofer, A. Klug, G. Trimmel, E.J.W. List, Influence of the bridging atom in fluorene analogue low-bandgap polymers on photophysical and morphological properties of copper indium sulfide/polymer nanocomposite solar cells, J. Polym. Sci. Part B Polym. Phys. 51 (2013) 1400–1410, https://doi.org/10.1002/polb.23350.
[28] C. Yi, X. Gong, Toward high performance inverted polymer solar cells, Curr. Opin. Chem. Eng. 2 (2013) 125–131, https://doi.org/10.1016/j.coche.2012.09.001.
[29] C.E.V. de Moura, L.S. Roman, M.B. Casu, T. Chassé, M.L.M. Rocco, M. Glaser, C.F.N. Marchiori, A.B. Rocha, B.G.A.L. Borges, Y. Garcia-Basabe, Electronic and structural properties in thermally annealed PSiF-DBT:PC71bm blends for organic photovoltaics, Thin Solid Films 615 (2016) 165–170, https://doi.org/10.1016/j.tsf.2016.07.012.
[30] J. Hou, H. Chen, S. Zhang, G. Li, Y. Yang, Synthesis, characterization, and photovoltaic properties of a low band gap polymer based on silole-containing polythiophenes and 2,1,3-Benzothiadiazole, J. Am. Chem. Soc. 130 (2008) 16144–16145, https://doi.org/10.1021/ja806687u.
[31] H. Zhou, L. Yang, S. Stoneking, W. You, A weak donor-strong acceptor strategy to design ideal polymers for organic solar cells, ACS Appl. Mater. Interfaces 2 (2010) 1377–1383, https://doi.org/10.1021/am1000344.
[32] V.S. Gevaerts, L.J.A. Koster, M.M. Wienk, A.J. Janssen, Discriminating between bilayer and bulk heterojunction polymer: fullerene solar cells using the external quantum efficiency, ACS Appl. Mater. Interfaces. 3 (2011) 3252–3255, https://doi.org/10.1021/am200755m.
[33] L. Cristina Wouk de Menezes, Y. Jin, L. Benatto, C. Wang, M. Koehler, F. Zhang, L. Stolz Roman, Charge transfer dynamics and device performance of environmentally friendly processed non-fullerene organic solar cells, ACS Appl. Energy Mater. 1 (2018) 4776–4785, https://doi.org/10.1021/acsaem.8b00884.
[34] L.A.A. Pettersson, L.S. Roman, O. Inganäs, Modeling photocurrent action spectra of photovoltaic devices based on organic thin films, J. Appl. Phys. 86 (1999) 487–496, https://doi.org/10.1063/1.370757.
[35] S.-.S. Sun, N.S. Sariciftci, Organic Photovoltaics: Mechanisms, Materials and Devices / [ed] Sam-Shajing Sun, Niyazi Serdar Sariciftci, Boca Raton, FL, CRC Press, USA, 2005, https://doi.org/10.1007/978-3-662-05187-0.
[36] J.D. Kotlarski, P.W.M. Blom, L.J.A. Koster, M. Lenes, L.H. Slooff, Combined optical and electrical modeling of polymer: fullerene bulk heterojunction solar cells, J. Appl. Phys. (2008) 103, https://doi.org/10.1063/1.2905243.
[37] L.A.A. Pettersson, S. Ghosh, O. Ingan, Optical anisotropy in thin films of poly (3, 4-ethylenedioxythiophene)–poly (4-styrenesulfonate), Org. Electron. 3 (2002) 143–148, https://doi.org/10.1016/S1566-1199(02)00051-4.
[38] E. Sader, A. Sayyed-Ahmad, Design of an optical water pollution sensor using a single-layer guided-mode resonance filter, Photonic Sens. 3 (2013) 224–230, https://doi.org/10.1007/s13320-013-0105-8.
[39] H.C. Andersen, Molecular dynamics simulations at constant pressure and/or temperature, J. Chem. Phys. 72 (1980) 2384–2393, https://doi.org/10.1063/1.439486.
[40] M. Elstner, P. Hobza, T. Frauenheim, S. Suhai, E. Kaxiras, P. Hobza, Hydrogen bonding and stacking interactions of nucleic acid base pairs: a density-functional-theory based treatment hydrogen bonding and stacking interactions of nucleic acid base pairs : a density-functional-theory based treatment, J. Chem. Phys. 114 (2001) 5149–5155, https://doi.org/10.1063/1.1329889.
[41] B. Aradi, B. Hourahine, DFTB+, a sparse matrix-based implementation of the DFTB method, J. Phys. Chem. A. 111 (2007) 5678–5684, https://doi.org/10.1021/jp070186p.
[42] F. Neese, The ORCA program system, Wiley Interdiscip. Rev. Comput. Mol. Sci. 2 (2012) 73–78, https://doi.org/10.1002/wcms.81.
[43] J.-.D. Chai, M. Head-Gordon, Long-range corrected hybrid density functionals with damped atom–atom dispersion corrections, Phys. Chem. Chem. Phys. 10 (2008) 6615–6620, https://doi.org/10.1039/b810189b.
[44] S. Few, J.M. Frost, J. Kirkpatrick, J. Nelson, Influence of chemical structure on the charge transfer state spectrum of a polymer:fullerene complex, J. Phys. Chem. C. 118 (2014) 8253–8261, https://doi.org/10.1021/jp412449n.
[45] L. Benatto, C.F.N. Marchiori, M.G.E. da Luz, M. Koehler, Electronic and structural properties of fluorene–thiophene copolymers as function of the composition ratio between the moieties: a theoretical study, Phys. Chem. Chem. Phys. 20 (2018) 20447–20458, https://doi.org/10.1039/C8CP02622J.
[46] M. Frisch, G.W. Trucks, H.B. Schlegel, G.E. Scuseria, M.A. Robb, J.R. Cheeseman, G. Scalmani, V. Barone, B. Mennucci, Ga. Petersson, Gaussian 09, revision a. 02, others Gaussian, Inc.,, Wallingford, CT, 2009, p. 200.
[47] Y. Garcia-Basabe, C.F.N. Marchiori, B.G.A.L. Borges, N.A.D. Yamamoto, A.G. Macedo, M. Koehler, L.S. Roman, M.L.M. Rocco, Electronic structure, molecular orientation, charge transfer dynamics and solar cells performance in donor/acceptor copolymers and fullerene: experimental and theoretical approaches, J. Appl. Phys. 115 (2014) 134901, , https://doi.org/10.1063/1.4870470.
[48] A. Köhler, D.A. dos Santos, D. Beljonne, Z. Shuai, J.-L. Brédas, A.B. Holmes, A. Kraus, K. Müllen, R.H. Friend, Chargeseparation in localizedanddelocalized electronic states in polymeric semiconductors, Nature 392 (1998) 903–906, https://doi.org/10.1038/31901.
[49] L. Benatto, M. Koehler, Effects of fluorination on exciton binding energy and charge transport of π-conjugated donor polymers and the ITIC molecular acceptor: a theoretical study, J. Phys. Chem. C. 123 (2019) 6395–6406, https://doi.org/10.1021/acs.jpcc.8b12261.
[50] L. Benatto, C.F.N. Marchiori, C.M. Araujo, M. Koehler, Molecular origin of efficient hole transfer from non-fullerene acceptors: insights from first-principles calculations, J. Mater. Chem. C. 7 (2019) 12180, https://doi.org/10.1039/C9TC03563J.
[51] C.F.N. Marchiori, N.A.D. Yamamoto, C.F. Matos, J. Kujala, A.G. Macedo, F. Tuomisto, A.J.G. Zarbin, M. Koehler, L.S. Roman, Annealing effect on donor-acceptor interface and its impact on the performance of organic photovoltaic devices based on PSiF-DBT copolymer and C60, Appl. Phys. Lett. 106 (2015) 133301, , https://doi.org/10.1063/1.4916515.
[52] G. Orlandi, F. Negri, Electronic states and transitions in C60 and C70 fullerenes, Photochem. Photobiol. Sci. 1 (2002) 289–308, https://doi.org/10.1039/b200178k.
[53] N.R. Tummala, C. Sutton, S.G. Aziz, M.F. Toney, C. Risko, J.L. Bredas, Effect of solvent additives on the solution aggregation of phenyl-c61-butyl acid methyl ester (PCBM), Chem. Mater. 27 (2015) 8261–8272, https://doi.org/10.1021/acs.chemmater.5b03254.
[54] R.J. Hill, L.M.D. Cranswick, International union of crystallography commission on powder diffraction rietveld refinement round robin. II. Analysis of monoclinic ZrO2, J. Appl. Crystallogr. 27 (1994) 802–844, https://doi.org/10.1107/S0021889894000646.
[55] G.B.M. Vaughan, Y. Chabre, D. Dubois, Effect of stacking disorder on the orientational ordering transition of solid c60, Europhys. Lett. 31 (1995) 525–530, https://doi.org/10.1209/0295-5075/31/9/004.
[56] S. Pfuetzner, J. Meiss, A. Petrich, M. Riede, K. Leo, Improved bulk heterojunction organic solar cells employing C70 fullerenes, Appl. Phys. Lett. 94 (2009) 2007–2010, https://doi.org/10.1063/1.3148664.
[57] J. Sakai, T. Taima, T. Yamanari, K. Saito, Annealing effect in the sexithiophene:C70 small molecule bulk heterojunction organic photovoltaic cells, Sol. Energy Mater. Sol. Cells. 93 (2009) 1149–1153, https://doi.org/10.1016/j.solmat.2009.02.007.
[58] X. Xi, W. Li, J. Wu, J. Ji, Z. Shi, G. Li, A comparative study on the performances of small molecule organic solar cells based on CuPc/C60 and CuPc/C70, Sol. Energy Mater. Sol. Cells. 94 (2010) 2435–2441, https://doi.org/10.1016/j.solmat.2010.08.008.
[59] T.M. Kim, H.S. Shim, M.S. Choi, H.J. Kim, J.J. Kim, Multilayer epitaxial growth of lead phthalocyanine and C70 using CuBr as a templating layer for enhancing the efficiency of organic photovoltaic cells, ACS Appl. Mater. Interfaces 6 (2014) 4286–4291, https://doi.org/10.1021/am405946m.